1 June 2001

ELSEVIER

Optics Communications 192 (2001) 169–181

OPTICS COMMUNICATIONS

www.elsevier.com/locate/optcom

Space-variant polarization state manipulation with computer-generated subwavelength metal stripe gratings

Ze'ev Bomzon *, Vladimir Kleiner, Erez Hasman

Optical Engineering Laboratory, Faculty of Mechanical Engineering, Technion-Israel Institute of Technology, Haifa 32000, Israel

Received 4 January 2001; received in revised form 28 February 2001; accepted 21 March 2001

Abstract

A novel approach to the design and analysis of space-variant polarization elements using computer-generated subwavelength metal stripe gratings is presented. We demonstrate that by locally controlling the direction and period of the grating any desired space-variant polarization state manipulation can be obtained. We illustrate our approach with two distinct types of manipulators: space-variant polarizers and space-variant polarization state transformations. The elements were formed on GaAs as well as ZnSe substrates and designed for laser radiation at 10.6 μm. The results include full space-variant polarization calculations and measurements and show high-quality space-variant polarized beams with a polarization purity of over 99%. © 2001 Published by Elsevier Science B.V.

PACS: 42.25.Ja; 42.40.Jv; 42.79.Dj

Keywords: Subwavelength gratings; Metal stripe gratings; Space-variant gratings

1. Introduction

Metal wire gratings have been known as polarizers for many years [1–5], and their use can be traced back to Heinrich Hertz who in 1888 used them to test the properties of radiowaves [1]. When the period of a metal wire grating is much smaller than the incident wavelength, the grating acts as a polarizer, reflecting all of the light polarized parallel to the wires (TE polarized light), and transmitting only light polarized perpendicular to the wires (TM polarized light). This is only true for very small periods and its validity has been examined in several papers [2,4]. For larger periods, still of a subwavelength nature, this assumption is no longer true, and it is necessary to use vectorial solutions of the Maxwell equations to predict the behavior of such gratings. This is typically done using rigorous coupled wave analysis (RCWA) [6,7].

Metal stripe gratings are usually linear uniform gratings, which form homogeneous space-invariant polarizers. Sometimes however, a different polarization is required at each location. Such nonuniform space-variant polarization can be useful for polarization coding of data in optical communication [8], optical computers [9] and neural networks, material processing [10], tight focusing [11], polarimetry [12] and for particle trapping and acceleration [13].

* Corresponding author. Fax: +972-4-832-4533.
E-mail address: zbomzy@tx.technion.ac.il (Z. Bomzon).

0030-4018/01/$ - see front matter © 2001 Published by Elsevier Science B.V.
PII: S0030-4018(01)01196-8

Recently, we presented a novel approach for polarization state transformation based on space-variant subwavelength metal stripe gratings [14]. We showed that by determining the local direction as well as the period of the grating any desired space-variant polarization state could be obtained. However, our discussion was limited only to elements fabricated on GaAs, and was restricted to polarization state transformations involving circularly polarized light for laser radiation at 10.6 μm.

In this paper we present a comprehensive theoretical and experimental investigation of space-variant polarization state manipulation using computer-generated subwavelength metal stripe gratings. We extend our discussion to include two distinct types of manipulators; space-variant polarizers and space-variant polarization state transformations. In the case of polarizers, the incident polarization need not be well defined, and only the transmitted intensity is of interest. We show that by careful design, the transmission axis [15] [1] (the direction of incident polarization for which transmission is maximum) can be locally controlled in order to achieve sophisticated space-variant polarizers to be used for applications such as imaging polarimetry [16], and space-variant intensity manipulation. On the other hand, polarization state transformations are designed to transform a beam with either a specific space-invariant or a specific space-variant polarization, into a well-defined space-variant polarized beam. Although our methods enable good control of the polarization and transmission intensity, they do not allow complete independent control of the two, and they remain connected.

In addition, we also present a unique analysis method for space-variant polarization transformations. The method is based on the use of Jones calculus and RCWA, and enables a full space-variant polarization state analysis of the desired element.

We demonstrate our approach with specific computer-generated space-variant polarization state manipulation elements for laser radiation at 10.6 μm. The elements were fabricated on GaAs as well as on ZnSe wafers using computer-generated Lee-type binary chrome masks and photolithographic processing. The experimental results which were based on a complete space-variant Stokes parameters measurement revealed high-quality space-variant polarized beams. Furthermore, we have found that due to its lower refractive index, ZnSe may be preferable to GaAs for the realization of both polarizers and polarization state transformations. This is because the lower refractive index of ZnSe results in uniformity of the polarization properties over a larger range of periods.

2. Space-variant polarizers

Gratings are typically defined by a grating vector, perpendicular to the grating stripes. The grating vector can be expressed as,

$$\vec{\mathbf{K}}_g = K_0 \cos(\beta)\hat{\mathbf{x}} + K_0 \sin(\beta)\hat{\mathbf{y}}, \tag{1}$$

where K_0 is the spatial frequency of the grating, β is the direction of the vector and $\hat{\mathbf{x}}$, $\hat{\mathbf{y}}$ are the unit vectors along the x-axis and the y-axis respectively.

A space varying grating can therefore be described by the vector,

$$\vec{\mathbf{K}}_g = K_0(x,y)\cos(\beta(x,y))\hat{\mathbf{x}} + K_0(x,y)\sin(\beta(x,y))\hat{\mathbf{y}}, \tag{2}$$

for which the local period and direction vary as a function of x and y. In order for such a grating to be physically realizable in a continuous way, $\vec{\mathbf{K}}_g$ should be a conserving vector i.e. $\nabla \times \vec{\mathbf{K}}_g = 0$, or more explicitly,

$$\frac{\partial K_0}{\partial y}\cos(\beta) - K_0 \sin(\beta)\left[\frac{\partial \beta}{\partial y}\right] = \frac{\partial K_0}{\partial x}\sin(\beta) + K_0\cos(\beta)\left[\frac{\partial \beta}{\partial x}\right], \tag{3}$$

which is a necessary restraint on $K_0(x,y)$ for a continuous grating with a local groove direction

[1] "The transmission axis of a linear polarizer is defined with respect to a linearly polarized light beam normally incident on the face of the polarizer. The transmission axis defines the direction that the Jones vector must have for the actual gain to be maximized".

$\beta(x,y)$ to exist. Once the grating vector is determined, the grating function $\phi(x,y)$, can be found by integrating $\vec{\mathbf{K}}_g$ along any arbitrary path in the x–y plane so that $\nabla\phi = \vec{\mathbf{K}}_g$.

Eq. (3) shows that the local period of space-variant gratings cannot be arbitrarily determined, but depends on the space varying choice of β. In order to understand such gratings, we need to first determine the effect of the period has on the polarization qualities of such gratings. For this purpose we define the polarization contrast ratio (PCR) as,

$$P(\Lambda) = \frac{T_{TM}(\Lambda)}{T_{TE}(\Lambda) + T_{TM}(\Lambda)}, \tag{4}$$

where Λ is the period, T_{TE} is the zero-order transmission when the incident beam is TE polarized, and T_{TM} is the zero-order transmission for a TM polarized beam. If only TM polarized light is transmitted, $P = 1$, and if only TE polarized light is transmitted, $P = 0$. Thus the PCR provides a tool for defining the grating's efficiency as a polarizer. Note, that since the polarization of TE and TM beams remains unchanged when transmitted through the grating, and that since any polarization state can be seen as a combination of the two, the transmitted intensity for an arbitrary polarized beam must lye between T_{TE} and T_{TM}. This means that if the PCR is greater than 0.5, larger transmission is achieved for TM polarized light, and that if it is smaller than 0.5, the larger transmission occurs for TE polarization.

In order to investigate the dependence of the PCR and of the transmission axis [15] [1] on period and substrate, we fabricated chirped gratings on GaAs and ZnSe. The gratings had dimensions of 5 mm × 7.5 mm, and are described by the grating vector,

$$\vec{\mathbf{K}}_g = \frac{2\pi}{\Lambda(x)}\hat{\mathbf{x}} = \frac{2\pi}{\Lambda_0 + bx}\hat{\mathbf{x}}, \tag{5}$$

where the local period varies linearly at a rate of $b = 0.4$ μm/mm in the x-direction, from $\Lambda(x = 0) = \Lambda_0 = 2$ μm to $\Lambda(x = 7.5\text{ mm}) = 5$ μm. The gratings were fabricated with a duty cycle of 0.55. To realize the gratings, a chrome mask was fabricated using high-resolution laser lithography. The grating was then transferred onto the substrate by use of AZ 5214 photoresist. The metal stripes were then realized using a lift-off technique. The GaAs substrate consisted of a semi-insulating wafer 500 μm thick, and the ZnSe substrate was a 2 mm thick window. The metal stripes consisted of a 10 nm layer of Ti, coated by 60 nm of Au. An anti-reflection coating was applied to the backside of the elements.

The experimental setup for measuring the intensity transmitted through the chirped gratings was as follows. Linearly polarized light at a wavelength of 10.6 μm was emitted from a CO_2 laser, and then passed through an additional polarizer, to ensure the polarization purity. This was followed by a half-wave plate, which enabled rotation of the incident polarization without energy loss. The beam was then expanded and projected onto the chirped grating of interest. The transmitted beam was magnified through a lens, and the grating was imaged onto a Spiricon Pyrocam 1. We then calculated the average intensity for each row of pixels in the y-direction, obtaining an average of the transmitted intensity at each local period. We repeated the measurement for TE and TM polarized beams, and then calculated the PCR.

The calculated and measured PCRs for both the ZnSe and GaAs gratings are shown in Fig. 1. The calculations were done using RCWA and a complex refractive index of $8.52 + 75.394i$ was used for the gold stripes. The experimental results, are in good agreement with the theory. Fig. 1 shows that when the period is small, the PCR for both gratings is close to 1, and for any incident beam, the transmitted light will be almost linearly polarized. However, as the period approaches λ/n, where $\lambda = 10.6$ μm is the wavelength and n is the refractive index of the substrate ($n = 3.27$ for GaAs and $n = 2.4$ for ZnSe), the PCR drops sharply reaching a minimum value of around 0.2. This minimum occurs at a period of $\lambda/n = 3.24$ μm for GaAs, and at a period of $\lambda/n = 4.4$ μm for ZnSe. At this point, most of the transmitted light is in fact TE polarized, and the grating works as a reverse polarizer [3]. After this dip, the merit function rises again to a value of around 0.6, and the grating no longer acts as an efficient polarizer. The location of the dips in both the GaAs and ZnSe,

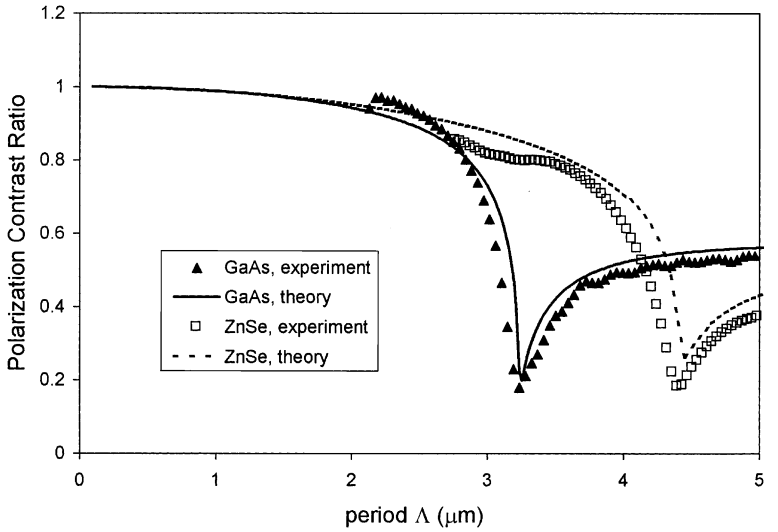

Fig. 1. Measured and calculated PCR for the ZnSe and GaAs chirped gratings as a function of the local period.

suggest that this phenomenon is strongly associated with the Wood anomaly [3].

Fig. 2 shows the transmission of TE and TM polarized light through the gratings described in Fig. 1. The measurements are in good agreement with the RCWA calculations. We note that for both the GaAs and the ZnSe gratings, when the period is much smaller than the wavelength, the TE transmission coefficient is close to zero. On the other hand, the TM transmission coefficient is

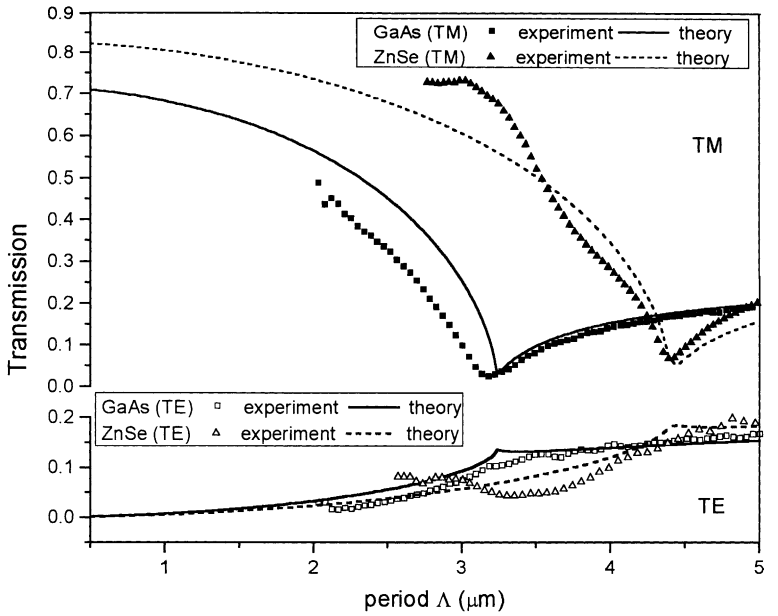

Fig. 2. Measured and calculated transmission for TE and TM polarized light incident on the GaAs and ZnSe chirped gratings as a function of the local period.

close to what could be expected at an interface between air and GaAs or ZnSe respectively as if there were no grating present (71% for GaAs 83% for ZnSe). This agrees with form birefringence theory [17,18], when using a complex refractive index for the metal stripes. This theory predicts that for very small periods, the TE polarized light will interact with the grating, as if it were a metal sheet, and that most of the TE polarized light will be reflected. As opposed to the TM polarized light which will behave as if no metal is present. However, our results also show that this approximation is valid for only a small range of periods, and that the TM transmission drops rapidly as the Wood anomaly is approached.

Figs. 1 and 2 suggest that it is advantageous to use substrates with low refractive indexes in order to construct polarizing metal stripe gratings, as this allows for higher efficiency and uniformity in the PCR over a larger range of periods, as well as resulting in higher transmission. It also presents a technological advantage, because it is easier to realize gratings with larger periods. However, the use of certain substrates poses a technical problem, since suitable photolithographic processes are not always available.

Next, we apply the results of Fig. 1 to the design of space-variant polarizers. More specifically, we wish to create a grating for which the transmission axis is different at each point. By relating to Fig. 1 we find that, as long as the local period is smaller than λ/n, this axis will be parallel to the grating vector. We apply this to the design of a specific grating with a transmission axis that varies linearly along the x-direction, and is described by the vector,

$$\vec{\mathbf{K}}_{\mathrm{g}}(x,y) = K_0(x,y)\cos(ax)\hat{\mathbf{x}} + K_0(x,y)\sin(ax)\hat{\mathbf{y}}. \tag{6}$$

Incorporating Eq. (6) into Eq. (3) yields,

$$\frac{\partial K_0}{\partial y}\cos(ax) = \frac{\partial K_0}{\partial x}\sin(ax) + aK_0\cos(ax), \tag{7}$$

which can be solved by equating the coefficients for the $\cos(ax)$ and $\sin(ax)$ to zero independently, resulting in the grating vector,

$$\vec{\mathbf{K}}_{\mathrm{g}} = \frac{2\pi}{\Lambda_0}\exp(ay)\Big[\cos(ax)\hat{\mathbf{x}} + \sin(ax)\hat{\mathbf{y}}\Big], \tag{8}$$

where Λ_0 is the period at $y = 0$. This result leads to the grating function,

$$\phi(x,y) = \frac{2\pi}{a\Lambda_0}\sin(ax)\exp(ay). \tag{9}$$

We realized a Lee-type [19] binary chrome mask describing the grating function of Eq. (9) using high-resolution laser lithography. The amplitude transmission for such a Lee-type binary mask can be derived as,

$$t(x,y) = U_{\mathrm{s}}[\cos(\phi) - \cos(\pi q)], \tag{10a}$$

where U_{s} is the unit step function defined by,

$$U_{\mathrm{s}}(\eta) = \begin{cases} 1, & \eta \geqslant 0 \\ 0, & \eta < 0 \end{cases}, \tag{10b}$$

and where q is the duty cycle of the grating. The mask is constructed so that where $t(x,y)$ is equal to one, the mask is chrome, and where $t(x,y)$ equals zero the mask is clear, so that it represents a binary description of the function ϕ. Note that although q does not affect the results of Eqs. (6)–(9), it does affect the transmission and the PCR. We studied the effect of q on these parameters, and found that there is a broad optimum at $q = 0.5$, and therefore realized the mask with this duty cycle.

Following the mask fabrication, the mask was transferred onto the desired substrate and the element was realized using the lift-off technique described previously for the chirped gratings. The space-variant grating was realized on both, a 500 μm thick GaAs wafer and on a 2 mm thick ZnSe window. The GaAs grating was restricted to a 5 mm × 3 mm rectangle with $a = -18°/\mathrm{mm}$, and $\Lambda_0 = 2$ μm so that $-90° < \beta < 0°$ and $2 < \Lambda < 5.1$ μm. On the ZnSe, the element consisted of a 5 mm × 2 mm rectangle, with $a = -18°/\mathrm{mm}$ and $\Lambda_0 = 2.8$ μm so that $2.8 < \Lambda < 5.1$ μm. For both gratings the fabrication procedure resulted in a duty cycle of 0.55, with the metal stripes consisting of an adhesion layer of 10 nm Ti, and a layer of 60 nm Au. An anti-reflection coating was applied to the backside of the gratings. Fig. 3 shows the magnified geometry of such a computer-generated mask with the resulting transmission axis varying

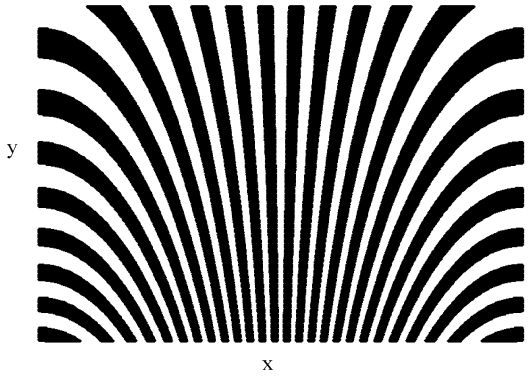

Fig. 3. Illustration of the magnified geometry of a computer-generated space-variant polarizer for which the orientation of the transmission axis rotates in the x-direction from 0° to 180°.

in the x-direction from 0° to 180°. The continuity of the grating can be clearly observed.

Using the experimental setup described earlier, we illuminated the grating with linearly polarized light. By rotating the half-wave plate, we could change the angle of polarization of the incoming beam, and locate the transmission axis along the element. Fig. 4 describes the direction of the transmission axis as a function of the x-coordinate of the element. The measurement was performed over the region of periods prior to the Wood anomaly. We see that for both the GaAs and the ZnSe space-variant gratings the direction of the transmission axis varies linearly along the x-axis with a slope of 18°/mm, in agreement with the theory.

We also examined the transmitted intensity distribution across the grating for a linearly polarized beam. For such illumination, the transmission is,

$$T = T_{\mathrm{TM}} \cos^2(\alpha) + T_{\mathrm{TE}} \sin^2(\alpha), \tag{11a}$$

where α is the angle between the electric field and the grating, and T_{TM} and T_{TE} are the period dependant transmission coefficients for TM and TE polarized light respectively. For a beam linearly polarized in the x-direction, and incident on the space-variant grating in discussion, this intensity distribution will be,

$$T(x,y) = T_{\mathrm{TM}}(y) \cos^2(ax) + T_{\mathrm{TE}}(y) \sin^2(ax), \tag{11b}$$

and for an incident beam polarized in the y-direction this will translate to,

$$T(x,y) = T_{\mathrm{TM}}(y) \sin^2(ax) + T_{\mathrm{TE}}(y) \cos^2(ax). \tag{11c}$$

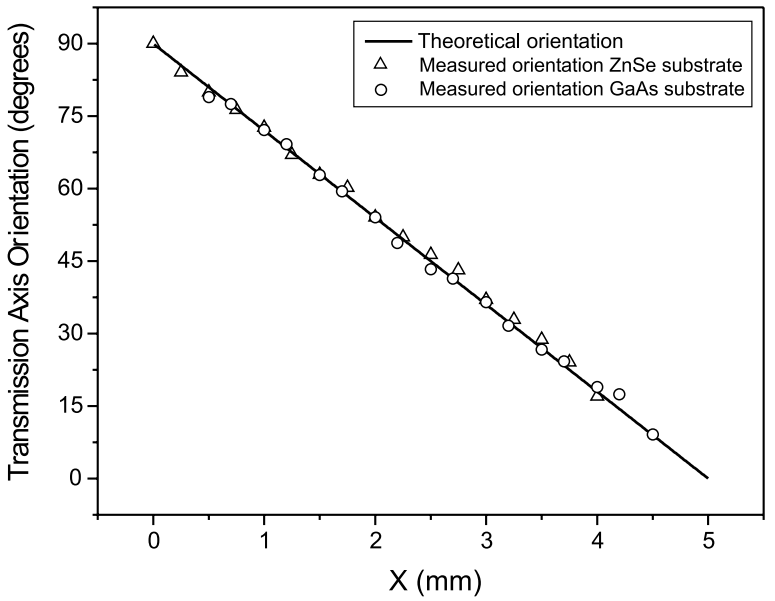

Fig. 4. Orientation of the transmission axis for the GaAs and ZnSe space-variant polarizers.

Fig. 5 shows the transmitted intensity distributions as a function of the x-coordinate for incident light linearly polarized in the x-direction as well as for incident light linearly polarized in the y-direction. The graph shows the average intensity measured at each x-coordinate over a small range of periods. For GaAs (Fig. 5(a)) this portion covered a range of periods 2.4–2.8 μm, and for ZnSe (Fig. 5(b)) the range was 3.2–3.45 μm. The experimental results fit the RCWA calculations, and the transmitted intensity is distributed as we expected.

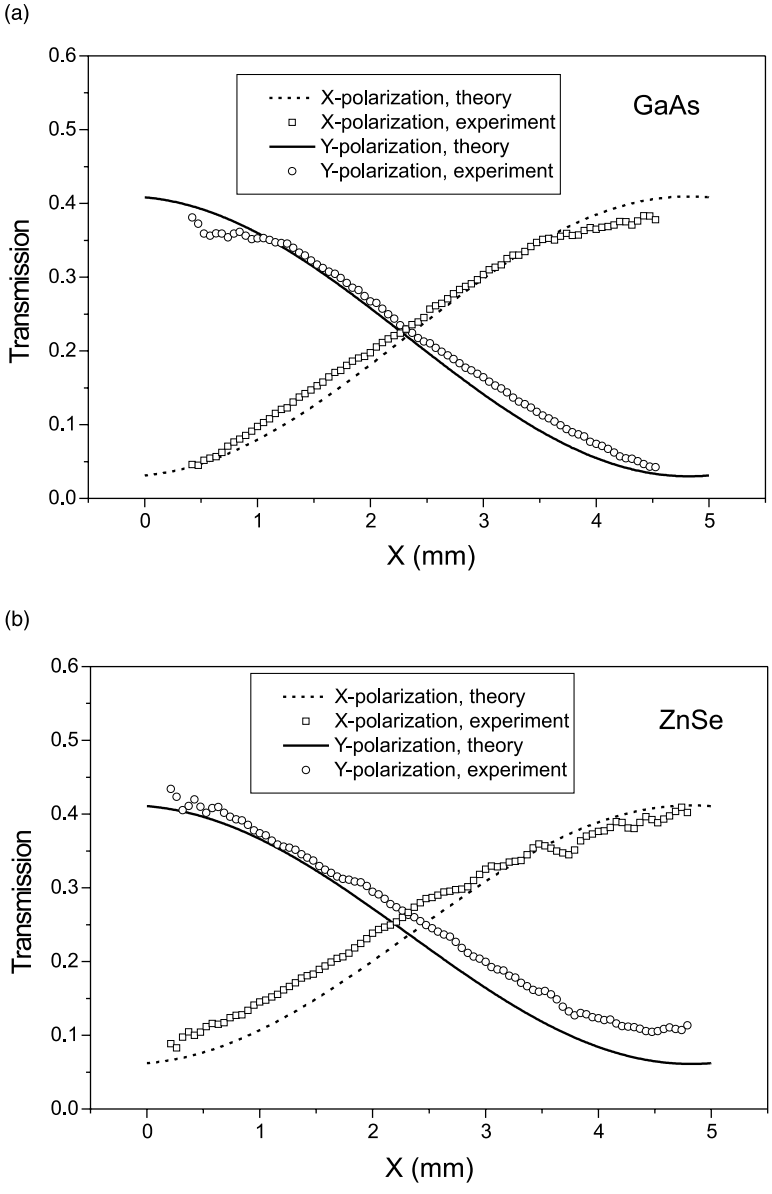

Fig. 5. Transmitted intensity distribution through (a) the GaAs space-variant polarizer, and (b) the ZnSe space-variant polarizer, for incident light linearly polarized in the x and y-directions.

3. Space-variant polarization state transformations

Until now, we have shown the construction of space-variant polarizers for which only the transmitted intensity is of interest. However, we have not yet related to the exact polarization state of the transmitted beam. Since a certain amount of TE polarized light is transmitted through the grating, it can be expected that the resulting beam will generally not be TM polarized. This can be important for applications such as atom trapping [13] or tight focusing [11], where the exact polarization state is important. We therefore commence with a method for the design of metal wire gratings for obtaining specific space-variant polarization wavefronts. In order to do so, we first study the effect of period and substrate properties on the resulting polarization.

Fig. 6 describes the polarization of light transmitted through a space-invariant grating. For such a grating, the transmitted field will generally be elliptically polarized. This ellipse can be defined by the azimuthal angle, ψ, which is the angle between the x-axis and the large axis of the ellipse, and the ellipticity, χ, where $\tan(\chi) = b/a$ is the ratio between the two axis's of the ellipse [20]. We define an additional angle $\Delta\psi$ as the angle between the large axis of the ellipse and the grating vector.

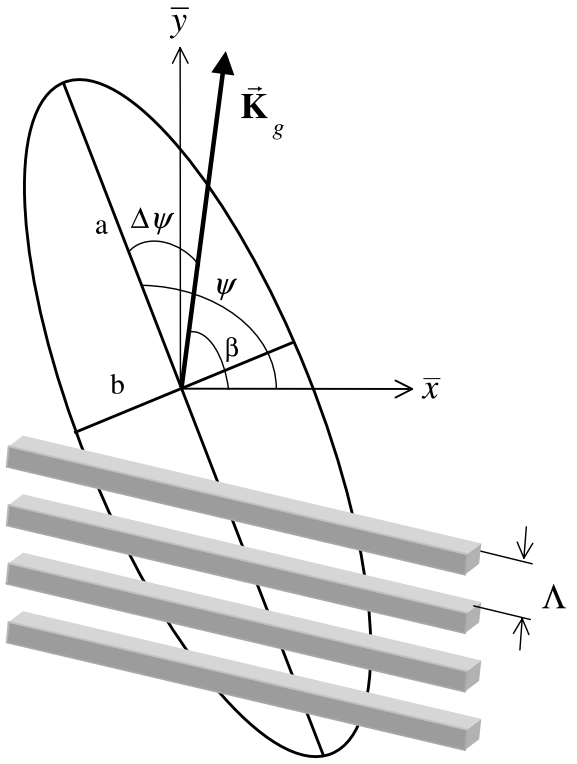

Fig. 6. Geometrical parameters of the polarization ellipse of light transmitted through a subwavelength grating.

In order to determine the dependence of $\Delta\psi$ and the ellipticity, $\tan(\chi)$, on the period of the grating, we calculated and measured the Stokes parameters [20] of the transmitted beam for the chirped gratings when the incident beam was circularly polarized. We chose the direction of the grating so that ψ and $\Delta\psi$ coincide. The experimental Stokes parameters were derived from four intensity measurements. For the first three, the transmitted light was passed through a polarizer with its axis oriented at 0° ($I_{0,0}$), at 90° ($I_{90,0}$) and at 45° ($I_{45,0}$). The fourth measurement was made by orienting the polarizer at 45°, and inserting a quarter-wave plate, with its fast axis at 0° between the polarizer and the element ($I_{45,90}$). The Stokes parameters were then calculated as,

$$S_0 = I_{0,0} + I_{90,0}, \tag{12a}$$

$$S_1 = I_{0,0} - I_{90,0}, \tag{12b}$$

$$S_2 = 2I_{45,0} - S_0, \tag{12c}$$

$$S_3 = S_0 - 2I_{45,90}. \tag{12d}$$

The azimuthal angle and ellipticity were then derived from the Stokes parameters according to the equations [20],

$$\tan(2\psi) = S_2/S_1, \tag{13a}$$

$$\sin(2\chi) = S_3/S_0. \tag{13b}$$

Fig. 7 shows a comparison between the azimuthal angle and the ellipticity of circularly polarized light at a wavelength of 10.6 μm transmitted through the GaAs and ZnSe chirped gratings. Fig. 7(a) shows the local azimuthal angle for both gratings, whereas Fig. 7(b) shows their ellipticity. Both ellipticity and azimuth display strong dependence on the period of the grating. In the region where the period is much smaller than the incident wavelength, ψ and $\tan(\chi)$ are close to

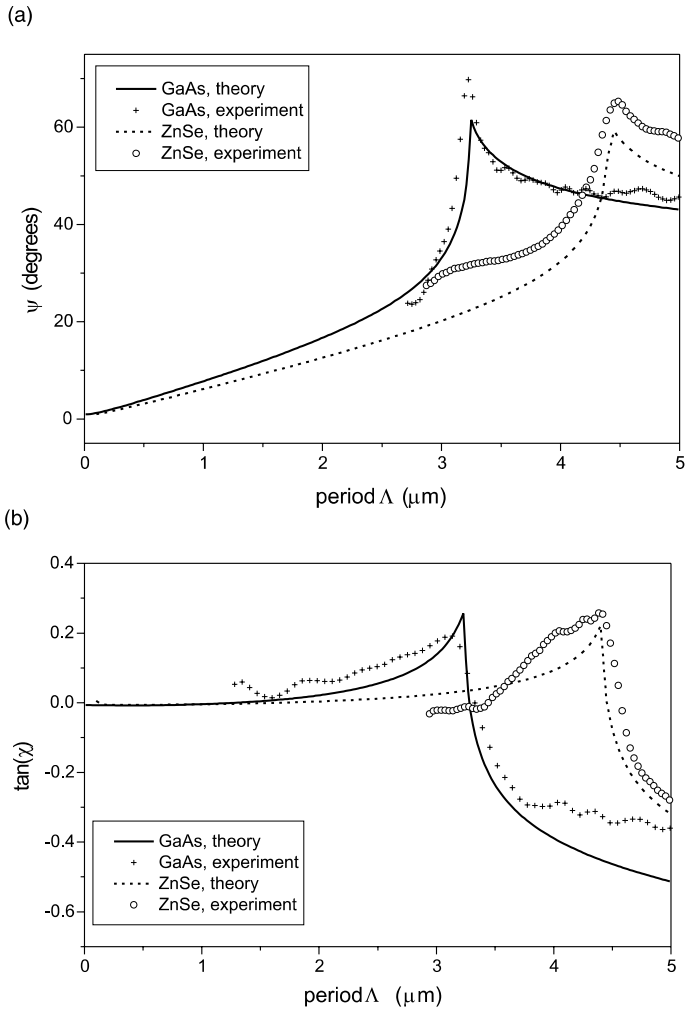

Fig. 7. Measured and calculated results for (a) the azimuthal angle ψ, and (b) the ellipticity, $\tan(\chi)$, of light transmitted through the chirped ZnSe and GaAs gratings as a function of the local period.

zero, for both the GaAs and the ZnSe polarization gratings, and the transmitted beam is nearly linearly polarized parallel to the grating vector. However, as the period becomes larger, the azimuthal angle and ellipticity increase. When the period approaches λ/n where λ is the wavelength and n is the refractive index of the substrate ($\lambda/n = 3.24$ for GaAs, $\lambda/n = 4.4$ for ZnSe), we observe a sharp increase in azimuthal angle and in ellipticity, in connection with the Wood anomaly. As evident, the theoretical results are well supported by the measurements.

Based on the dependence of the azimuthal angle on the period of the grating, we conclude that in order to transform circularly polarized light into a beam with a local azimuthal of ψ, the local grating direction should be period dependent and can be expressed as,

$$\beta(x,y) = \psi(x,y) - \Delta\psi(K_0(x,y)). \tag{14}$$

This can then be applied to the grating condition in Eq. (3) to obtain a new self-containing grating equation,

$$\frac{\partial K_0}{\partial y}\cos(\beta) - K_0\sin(\beta)\left[\frac{\partial \psi}{\partial y} - \frac{\partial \Delta\psi}{\partial K_0}\frac{\partial K_0}{\partial y}\right] = \frac{\partial K_0}{\partial x}\sin(\beta) + K_0\cos(\beta)\left[\frac{\partial \psi}{\partial x} - \frac{\partial \Delta\psi}{\partial K_0}\frac{\partial K_0}{\partial x}\right]. \tag{15}$$

We emphasize that in order for a grating to satisfy this equation, the grating direction cannot be chosen independent of the period, but that they are strongly connected. This is opposed to our initial design procedure for polarizers in which the grating direction was determined freely, and only the period was subject to restraint. We now apply Eq. (15) in order to obtain a grating for transforming circularly polarized light into a beam with an azimuthal angle that varies linearly in the x-direction. For such an operator, the local grating direction should be,

$$\beta(x,y) = ax - \Delta\psi(K_0(x,y)). \tag{16}$$

We notice that, under the zero-order approximation that $\Delta\psi = \psi_0 = \text{const}$, this results in the grating described by Eq. (8). Fig. 8 shows the experimental azimuthal angle of the beam transmitted through the previously discussed ZnSe space-variant grating, while illuminated with circularly polarized light with a wavelength of 10.6 μm. For constant y (i.e. constant period), the azimuthal angle varies linearly in the x-direction over a range of 90°, as expected. However there is also an unwanted variation of the azimuthal angle in the y-direction, as the period increases. This is due to the insufficiency of the zero-order approximation in describing the dependence of $\Delta\psi$ on period. The insufficiency of this approximation is highlighted by Fig. 7(a), which describes a much more complex dependence of azimuthal angle on period.

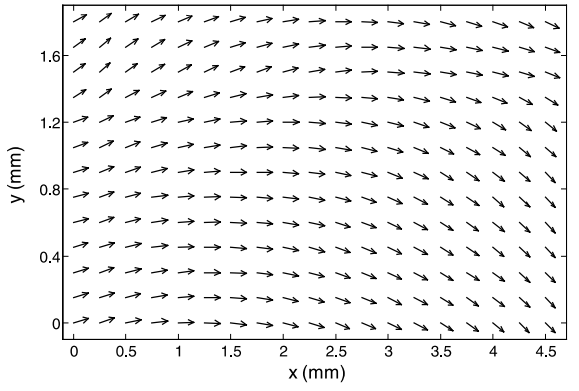

Fig. 8. Experimental measurement of the polarization of light transmitted through the ZnSe space-variant polarization state transformation element, when illuminated with circularly polarized light. The arrows indicate the azimuthal angle of the transmitted beam.

The performance of a space-variant subwavelength grating can be theoretically verified. For this purpose we present a full space-variant polarization analysis. The method is based on RCWA and a Jones representation of the grating. We observe that, the Jones matrix for a subwavelength grating described by the vector, $\vec{\mathbf{K}}_g = (2\pi/\Lambda)\hat{\mathbf{x}}$ is,

$$\hat{\mathbf{J}}(\Lambda) = \begin{bmatrix} e_{xx} & 0 \\ 0 & e_{yy} \end{bmatrix}, \tag{17}$$

where

$$\vec{E}_x = \begin{bmatrix} e_{xx} \\ 0 \end{bmatrix} \tag{18a}$$

and

$$\vec{E}_y = \begin{bmatrix} 0 \\ e_{yy} \end{bmatrix} \tag{18b}$$

are the complex Jones vectors for the transmitted fields for incident light, linearly polarized in the x-direction and in the y-direction respectively. These fields can be calculated using RCWA, and once the matrix has been constructed, the Jones vector of the transmitted field for any incident polarization can be found as

$$\vec{\mathbf{E}}_{out} = \hat{\mathbf{J}}\vec{\mathbf{E}}_{in}. \tag{19}$$

Furthermore, the Jones matrix for the same grating rotated at an arbitrary angle β can be calculated as

$$\hat{\mathbf{J}}_{Rot} = M(\beta)\hat{\mathbf{J}}M^{-1}(\beta), \tag{20}$$

where

$$M(\beta) = \begin{bmatrix} \cos\beta & -\sin\beta \\ \sin\beta & \cos\beta \end{bmatrix} \tag{21}$$

is the 2×2 rotation matrix. Note, that $\hat{\mathbf{J}}_{Rot}$ is no longer a diagonal matrix. Applying Eq. (20) to space-variant elements, in which the period and

direction vary in the x–y plane, we find that such operators take the form of,

$$\hat{\mathbf{J}}(x,y) = M(\beta(x,y))\hat{\mathbf{J}}(\Lambda(x,y))M^{-1}(\beta(x,y)), \qquad (22)$$

which is a simple and elegant method for representing space-variant polarization gratings, enabling calculation of the transmitted field for any arbitrary incident polarization. The Stokes parameters can then be calculated from the Jones vector by use of the coherence matrix [21].

Fig. 9 shows cross-sections of the measured and calculated ellipticity ((a) and (b)) and azimuthal angle ((c) and (d)) across the GaAs and ZnSe space-variant elements respectively. The calculations were done using the method described by Eq. (22), and the good coincidence between the experimental results and the calculations confirms the validity of our Jones calculus based calculation method. Examination of Fig. 9(a) and (b) shows constant ellipticity for constant y, regardless of the direction of the grating, as expected. Whereas the azimuthal angle in Fig. 9(c) and (d) follows straight parallel lines, indicating a linear variation of 90° across the element, and also highlighting the variation of the azimuthal angle with period. This variation can be reduced by higher order solutions of Eq. (15). By applying a perturbation method to the solution of Eq. (15), we found that a first-order correction may simply be obtained by rotating the element. Numerical simulations using RCWA and full space-variant polarization analysis based on Eq. (22), yield an optimal rotation angle of 36° for the ZnSe and 30° for the GaAs element. Fig. 10 shows the measured and calculated variation of the azimuthal angle along the x-axis for a small portion of the ZnSe element when rotated by 36°. The portion consists of a 5 mm × 0.9 mm strip with periods from 3 to 4 μm. The graph shows a

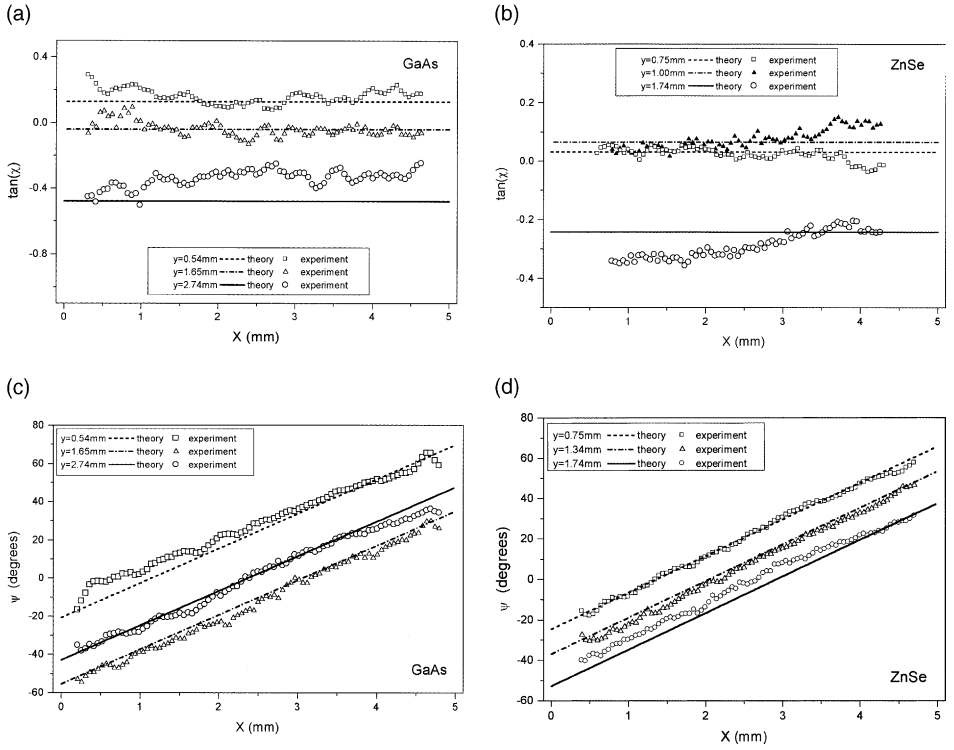

Fig. 9. Experimental and calculated cross-sections of the polarization for circularly polarized light transmitted through the GaAs and ZnSe space-variant polarization state transformation elements. The graphs show the ellipticity, tan(χ), for (a) the GaAs and (b) the ZnSe elements, as well as the azimuthal angle, ψ, for (c) the GaAs and (d) the ZnSe elements.

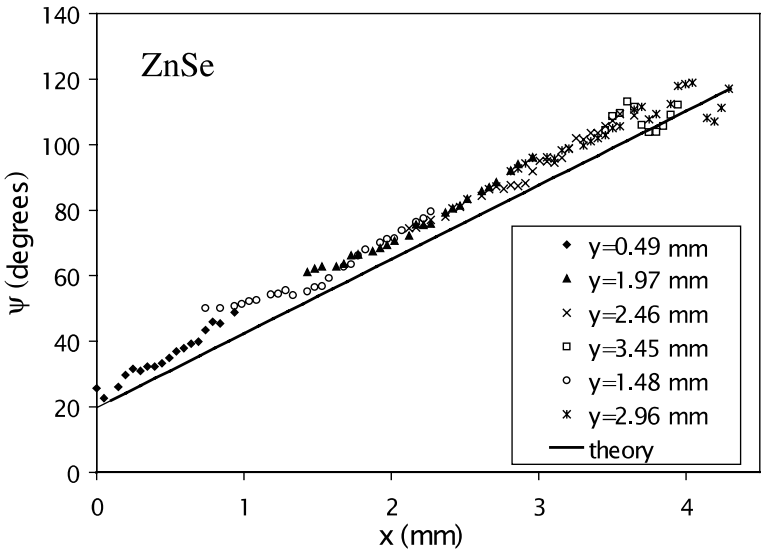

Fig. 10. Measured and calculated azimuthal angle as a function of x-location for some y-coordinates, of the ZnSe space-variant polarization state transformation element when rotated by 36°. Note that the large values of y, result from the geometry of the revolved thin strip.

linear variation of the azimuthal angle along the x-axis and very little variation in the y-direction, with good agreement between experiment and calculation. The calculated results revealed an average deviation of the azimuthal angle from a linear curve 0.6° and the experimental deviation was 3.2°. Additionally, taking into account an average ellipticity of 3.5°, reveals an overall polarization purity (percentage of power which is polarized in the desired direction) of 99.2%. A similar GaAs element yielded an average ellipticity of 6° and an overall polarization purity of 98.6%.

4. Concluding remarks

To conclude, we have shown a novel approach to the design and analysis of space-variant polarizing elements using metal stripe gratings, whereby locally controlling the direction and period of the grating any desired space-variant manipulation can be obtained. We have demonstrated the design of space-variant polarizers and of space-variant polarization state transformations and have shown that such manipulators are capable of producing high polarization purity of over 99%. Furthermore, we have studied metal stripe gratings on ZnSe and GaAs and found that due to its lower refractive index, the use of ZnSe substrates results in a higher PCR, and in a lower ellipticity for the transmitted beam than those of GaAs. This suggests that future work should focus on the use of low refractive index substrates, in order to overcome the limitations posed by the Wood anomaly, as well as on the realization of more intricate designs.

Acknowledgements

The authors are grateful to Svetlana Yofis for her help and professional advice in perfecting the photolithographic processing.

References

[1] H. Hertz, Electric Waves, Macmillan, New York, 1893.
[2] E.N. Glytiss, T.K. Gaylord, Appl. Opt. 31 (1992) 4459–4470.

[3] M. Honkanen, V. Kuittinen, J. Lautanen, J. Turunen, B. Schnabel, F. Wyrowski, Appl. Phys. B 68 (1999) 81–85.
[4] B. Schnabel, E.B. Kley, F. Wyrowski, Opt. Eng. 38 (1999) 220–226.
[5] S. Astilean, Ph. Lalanne, M. Palamaru, Opt. Commun. 175 (2000) 265–273.
[6] M.G. Moharam, T.K. Gaylord, J. Opt. Soc. Am. A 3 (1986) 1780–1787.
[7] P. Lalanne, G.M. Morris, J. Opt. Soc. Am. A 13 (1996) 779–784.
[8] B. Javidi, T. Nomaru, Opt. Eng. 39 (2000) 2439–2443.
[9] N. Davidson, A.A. Friesem, E. Hasman, Appl. Opt. 31 (1992) 1810–1812.
[10] V.G. Niziev, A.V. Nesterov, J. Phys. D 32 (1999) 1455–1461.
[11] S. Quabis, R. Dorn, M. Eberler, O. Glöckl, G. Leuchs, Opt. Commun. 179 (2000) 1–7.
[12] C. Someda, Opt. Lett. 24 (1999) 1657–1659.
[13] Y. Liu, D. Cline, P. He, Nucl. Instrum Meth. Phys. Res. A 424 (1999) 296–303.
[14] Z. Bomzon, V. Kleiner, E. Hasman, Opt. Lett. 26 (2001) 33–35.
[15] C. Brosseau, Fundamentals of Polarized Light, Wiley, New York, 1998.
[16] G.P. Nordin, J.T. Meier, P.C. Meier, P.C. Deguzman, M.W. Jones, J. Opt. Soc. Am. A 16 (1999) 1168–1174.
[17] M. Born, E. Wolf, Principles of Optics, seventh ed., Cambridge University Press, Cambridge, 1999.
[18] P. Yeh, Opt. Commun. 26 (1978) 289–292.
[19] W.H. Lee, Appl. Opt. 13 (1974) 1677–1682.
[20] E. Collet, Polarized Light, Marcel-Dekker, New York, 1993.
[21] T. Carozzi, R. Karlsson, J. Bergman, Phys. Rev. E 61 (2000) 2024–2028.